Improvement in EEG Source Imaging Accuracy by Means of Wavelet Packet Transform and Subspace Component Selection

Dong Wang, Zhian Liu, Yi Tao, Wenjing Chen, Badong Chen, Qiang Wang, Xiangguo Yan, and Gang Wang, *Member, IEEE*

***Abstract*— The electroencephalograph (EEG) source imaging (ESI) method is a non-invasive method that provides high temporal resolution imaging of brain electrical activity on the cortex. However, because the accuracy of EEG source imaging is often affected by unwanted signals such as noise or other source-irrelevant signals, the results of ESI are often incongruous with the real sources of brain activities. This study presents a novel ESI method (WPESI) that is based on wavelet packet transform (WPT) and subspace component selection to image the cerebral activities of EEG signals on the cortex. First, the original EEG signals are decomposed into several subspace components by WPT. Second, the subspaces associated with brain sources are selected and the relevant signals are reconstructed by WPT. Finally, the current density distribution in the cerebral cortex is obtained by establishing a boundary element model (BEM) from head MRI and applying the appropriate inverse calculation. In this study, the localization results obtained by this proposed approach were better than those of the original sLORETA approach (OESI) in the computer simulations and visual evoked potential (VEP) experiments. For epilepsy patients, the activity sources estimated by this proposed algorithm conformed to the seizure onset zones. The WPESI approach is easy to implement achieved favorable accuracy in terms of EEG source imaging. This demonstrates the potential for use of the WPESI algorithm to localize epileptogenic foci from scalp EEG signals.**

Manuscript received August 8, 2020; revised February 8, 2021; accepted February 25, 2021. Date of publication March 9, 2021; date of current version March 16, 2021. This work was supported in part by the National Natural Science Foundation of China under Grant 32071372, Grant 31571000, Grant 61976175, Grant 61471291, and Grant 81201162; and in part by the Natural Science Basic Research Program of Shaanxi through the Program under Grant 2020JM-037. *(Corresponding author: Gang Wang.)*

Dong Wang, Zhian Liu, Yi Tao, Xiangguo Yan and Gang Wang are with the Key Laboratory of Biomedical Information Engineering of Ministry of Education, School of Life Science and Technology, Institute of Biomedical Engineering, Xi'an Jiaotong University, Xi'an 710049, China, also with the National Engineering Research Center for Healthcare Devices, Guangzhou 510500, China, and also with the Key Laboratory of Neuro-informatics and Rehabilitation Engineering of Ministry of Civil Affairs, Xi'an 710049, China (e-mail: ggwang@xjtu.edu.cn).

Wenjing Chen is with the Department of Neurosurgery, West China Hospital, Sichuan University, Chengdu 610041, China.

Badong Chen is with the Institute of Artificial Intelligence and Robotics, Xi'an Jiaotong University, Xi'an 710049, China.

Qiang Wang is with the Department of Anesthesiology and the Center for Brain Science, The First Affiliated Hospital of Xi'an Jiaotong University, Xi'an 710061, China.

Digital Object Identifier 10.1109/TNSRE.2021.3064665

***Index Terms*— EEG source imaging, wavelet packet transform, subspace component selection, boundary element model, sLORETA.**

I. Introduction

SCALP electroencephalograph (EEG) is a non-invasive method to record brain electrical activity from large cohorts of neurons in the cerebral cortex [1], [2]. Since EEG contains important information on functional brain activity, these signals have been widely used clinically and in neuroscience research [3], [4]. In particular, EEG plays an extremely important role in seizure detection [5], [6], seizure prediction [7]–[9] and epileptogenic foci localization [10] for patients with refractory partial epilepsy. In addition to EEG, the neural activity of the brain can also be explored using many other noninvasive imaging methods, including functional magnetic resonance imaging (fMRI), functional near-infrared spectroscopy (fNIRs), single-photon emission computed tomography (SPECT) and positron emission tomography (PET). These functional imaging methods provide desirable spatial resolution, but fail to capture the real-time neural activities in the cerebral cortex. EEG source imaging (ESI) can be utilized to provide noninvasive imaging of the brain's neural activities. As long as scalp EEG measurements are available, ESI can estimate brain electrical activity with high temporal resolution by solving the so-called EEG inverse problem.

Given what is known about source models, head models, and EEG electrodes, the EEG inverse problem can be used to reconstruct the distribution of electrical sources within the brain via scalp EEG signals. The most widely used source models are parametric dipole models and distributed source models. Dipole models use the location and orientation parameters of equivalent current dipoles (ECD) to model focal sources in order to denote focal brain electrical activities. The multiple signal classification (MUSIC) algorithm recognizes the location and orientation of optimal ECD by scanning the entire source space and maximizing the scan metric of dipoles. RAP-MUSIC and FINE were proposed to improve the multiple-peak problem and spatial resolvability of the original MUSIC algorithm [11], [12]. Recent studies have emphasized the exploration of distributed source models. The low-resolution brain electromagnetic tomography (LORETA) and focal underdetermined system solver (FOCUSS) algorithms have been developed to obtain source imaging solutions with reasonable resolution and accuracy by incorporating various additional constraints as a priori information [13], [14]. For EEG source imaging, the head model has an impact on the EEG source imaging results. The most common head model is the three-or four-layer spherical head model. Because the spherical head model is extremely different from the model based on the realistic geometry of the head, the results of EEG source imaging are far from the actual current density distribution. Therefore, when choosing the realistic geometry head model based on the MRI images, the source imaging results will be close to the actual situation, which has important practical significance and clinical value [15]. In terms of the number of electrodes, the routine montage of 19-31 electrodes is able to localize the neural electrical activities at a sub-lobar level. However, many investigations have suggested that high-density montages provided improved source imaging accuracy as compared to low-density montages [16].

The ESI method has been applied to the tracking of changes in brain source dynamics, such as for brain-computer interfaces (BCIs) [17], [18], imaging of physiological activity [19], and epileptogenic foci localization [20], [21]. Rimpiläinen *et al.* proposed a Bayesian approximation error (BAE) framework for ESI when modelling unknown skull conductivity [22]. Mäkelä *et al.* introduced a new truncated TRAP-MUSIC method to accurately estimate the true number of brain-signal sources in computer simulations [23]. In the source imaging of physiological activity, Machado *et al.* employed the source imaging of P300 visual evoked potentials (VEPs) to investigate the cognitive processing functions in the visual cortices of healthy subjects [24]. Hedrich *et al.* evaluated the source localization of somatosensory evoked responses and compared four kinds of distributed source localization methods [25]. For clinical diagnostics and treatment of epilepsy, the standard methods include video EEG monitoring, structural MRI, and neuropsychological testing [26]–[29]. Although both interictal and ictal EEG signals can reflect the electrophysiological signatures of epileptiform activities, there are important differences between ictal and interictal source imaging in epilepsy [30], [31]. Lin *et al*. used independent component analysis (ICA) and LORETA to perform dynamic ictal imaging of brain epileptic activities with 76 non-invasive high-density EEGs [32]. Pellegrino *et al.* proposed a new non-invasive magnetic and electric source imaging method to localize the seizure onset zone using ictal MEG and EEG recordings [30]. Li *et al.* described a novel ESI method which uses cross-frequency coupled potential signals to localize the epileptogenic zone [33]. However, because ictal EEG signals are impacted by movement artifact and noise, there remain many challenges for dynamic ictal source imaging. Additionally, when monitoring long-term video EEG, interictal spike-wave activity is often observed in patients with medically intractable epilepsy. Hence, in recent years, many attempts have been made to use source imaging of interictal spikes for epileptogenic foci localization to aid in the presurgical evaluation of epilepsy [31], [34]. Gavaret *et al.* used the real boundary element head model and dipole model to localize the seizure onset zone with 64-channel interictal spike waves [35]. Strobbe *et al.* presented a multiple volumetric sparse priors (MSVP) approach to localize presurgical epileptogenic foci by means of interictal spikes [36]. Coito *et al.* proposed the fusion of ESI and directed functional connectivity to estimate the interictal epileptogenic zone location in patients with focal epilepsy [37].

However, in the above research, little attention was paid to the measurement signal itself. Scalp EEG signals present with many redundant frequency components that have no contribution to the desired neuron activities. These components can result in source imaging errors when calculating inverse problems. If these unrelated components are removed, the result of source localization may be improved. Wavelet packet transform (WPT) is a widely used time-frequency analysis method which can be used to remove redundant components and select more relevant subspaces [38]. In order to improve the accuracy of source imaging by means of noninvasive scalp EEG recordings, a novel ESI method (WPESI) based on WPT was proposed in the present study. Computer simulation and VEP data were used to quantitatively analyze the source imaging accuracy of the proposed method, and epileptic data were utilized to qualitatively evaluate the estimated epileptogenic zone.

II. Methods

A. ESI Based on WPT

A schematic diagram of the WPESI algorithm for EEG source imaging is provided in Fig. 1. The source-related EEG signals are firstly obtained by subspace component selection and WPT reconstruction. Then, the head model, which contains three compartments (i.e., skin, skull, and brain), is established with a realistic geometry boundary element model (BEM). Finally, the source distribution is achieved by solving the EEG inverse problem.

1) WPT of EEG Signals: WPT is an extension of wavelet transform (WT) and can be used to provide insight into EEG signals from the perspective of multi-resolution analysis. EEG recordings mainly contain delta band (0.5-4 Hz), theta band (4-8 Hz), alpha band (8-12 Hz), beta band (12-30 Hz) and gamma band (>30 Hz) signals. In order to separate these EEG rhythms from one another, EEG signals are usually decomposed by WPT. Assuming that the sampling rate of the EEG is f_s and the level of the wavelet packet analysis layer is l, the formula $f_s/2^{l+1} \leq 4$ must be satisfied given that the fact that the frequency of the last decomposition level is about 4 Hz. In this study, the l was selected as the smallest value that satisfied the above condition, and the Symlet wavelet of order 5 ($Sym5$) was used as the mother function to decompose and reconstruct each channel of the EEG signal using the MATLAB platform (MathWork, Natick, MA).

2) Subspace Component Selection: The subspace component signals were firstly reconstructed from each sub-band of wavelet packet coefficients. These signals, where the length of each signal was equal to the original signal, were arranged in the original EEG channel order to obtain multi-channel EEG in each subspace. The multichannel EEG generated by wavelet

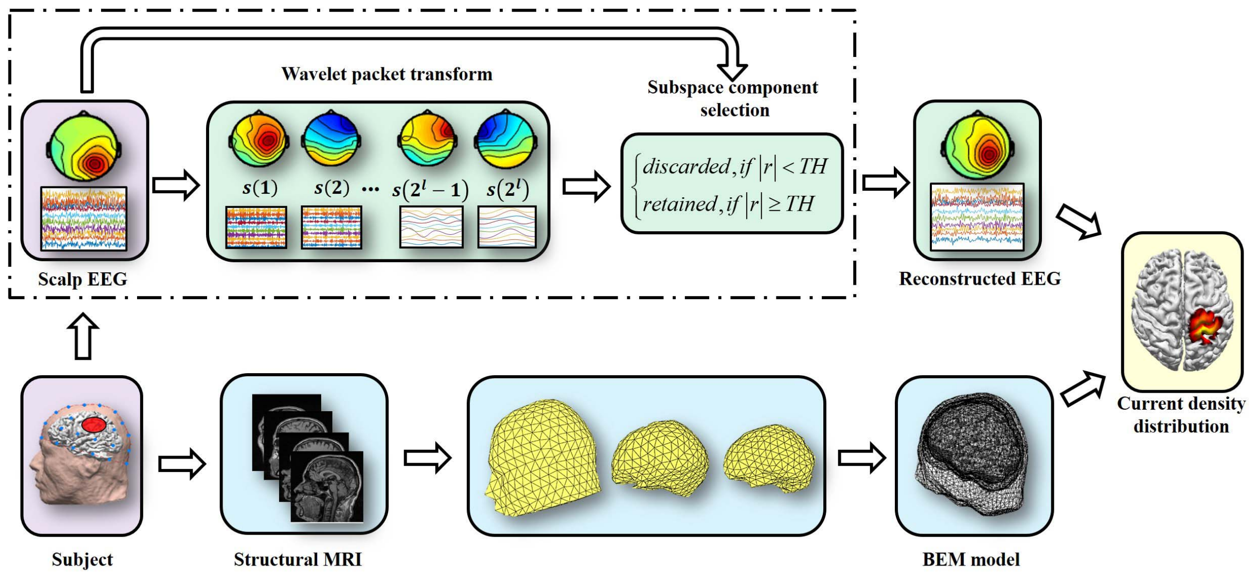

Fig. 1. Pipeline diagram of EEG source imaging based on wavelet packet transform and subspace component selection.

packet decomposition represents the different frequency bands of the EEG signal, which can be defined as the subspace components. Then, Pearson correlation coefficient analysis was performed and the subspace component with the highest absolute value correlation coefficient was selected. Assuming the subspace component at a certain time point is M and the original signal at the same time point is N, the Pearson correlation coefficient r satisfies the following formula:

$$r = \frac{\sum (M - \overline{M})(\mathrm{N} - \overline{N})}{\sqrt{\sum (M - \overline{M})^2 (\mathrm{N} - \overline{N})^2}} = \frac{l_{MN}}{\sqrt{l_{MM} l_{NN}}} \tag{1}$$

where r is the Pearson correlation coefficient between the subspace component and the original EEG signal in the time domain.

$$\begin{cases} discarded, & if \ |r| < TH \\ retained, & if \ |r| \geq TH. \end{cases} \tag{2}$$

After calculating the correlation coefficients between each subspace component and original EEG signals, the subspace components were screened. As shown in Formula (2), if the absolute value of a correlation r was small, which means that the difference in the topographic map between the subspace component and the original EEG signals was large, the subspace component was discarded. Finally, the retained subspace components were reconstructed to obtain the source-related EEG signals by WPT. In the following experiments, all thresholds *TH* were set to a constant value of 0.5.

3) Realistic Geometry Boundary Element Model (BEM): A dataset of anatomical magnetic resonance (MR) images from a human subject was used for the following computer simulation and VEP experiments. The MRI dataset (256 slices, a field of view of 256 mm, matrix size: 256×256, voxel size: $1 \times 1 \times 1$ mm^3) was acquired on a GE Signa machine. For the following epilepsy experiments, the BEM was built using these clinical MRI images. The analysis software Curry 6.0 (Neuroscan, Compumedics, Charlotte, NC, USA) was used to perform the contour extraction, smoothing and segmentation of all MRI images. For head modeling, the surfaces (skin layer, outer skull layer, and inner skull layer) were segmented from the MR images. The conductivities of the different tissues were assumed to be 0.33 S/m for the skin, 0.0165 S/m for the skull, and 0.33 S/m for the brain [39]. Then, the conductivity values were assigned to each of the compartments and a three-layer realistic geometry BEM was established. The solution space comprised around 25,000 current dipole sources which were evenly positioned on the folded cortical surface.

4) EEG Inverse Problem: The EEG inverse problem involves obtaining the source information of brain electrical activity by using the source-related EEG signals. The forward model used here is described in the following equation:

$$Y = GX + \varepsilon \tag{3}$$

where Y denotes the scalp EEG signals, X is the distributed sources on the cortical surface, ε represents white noise and G is the transfer matrix through which the EEG signals are linked with the distributed sources. The corresponding inverse problem was that X should be solved with known Y and G. However, obtaining this source information from noninvasive scalp EEG measurements is a large-scale underdetermined problem. Therefore, in order to obtain a reasonable source distribution, some restrictions on the EEG inverse solution should be considered. After choosing the reasonable parameters of the source model and head model, an accurate current density distribution can be obtained by using appropriate numerical calculations. Here, the standardized low-resolution brain electromagnetic tomography (sLORETA) algorithm was used [40], a common distributed source imaging method for neuroscience research [41]–[43], to solve the EEG inverse problem.

B. Simulated and Real EEG Signals

1) Computer Simulation Data: The simulated EEG signals were obtained by solving the EEG forward calculation according to the electrode montage, transfer matrix and the intensity and direction of dipole sources. The boundary element head model was also established in the simulation calculation. The electrode setting was based on the modified 10/20, 10/10 or 5/10 system configurations.

Both single dipole source and extended source were considered in the computer simulation. For the single dipole source, 50 dipole sources of different depths were placed over the folded cortical surface to represent the cortical neural activity. These dipole sources were randomly selected and sorted in terms of distance from the simulated dipole source to the central point of the brain, which was defined as the sphere center relative to all scalp electrode coordinates. Additionally, each dipole was assumed to have a random current intensity from 0 to 100 mA and all dipole sources were constrained to predefined orientations that were perpendicular to the local cortical patch. In the EEG forward calculation, these 50 dipole sources were used to generate the scalp EEG potentials. The Gauss white noise (GWN) and pink noise signals with certain signal-to-noise ratios (SNRs) were randomly generated 200 times. Then, these noise signals were superimposed to the generated scalp potentials to simulate 19, 32, 64 and 128 channels of noise-contaminated EEG signals. When 19 channels were employed, the chosen electrodes were Fp1, Fp2, F7, F3, Fz, F4, F8, T7, C3, Cz, C4, T8, P7, P3, Pz, P4, P8, O1 and O2. For 32 channels of EEG signals, Fp1, Fp2, F9, F7, F3, Fz, F4, F8, F10, FC3, FC4, T9, T7, C3, Cz, C4, T8, T10, A1, CP5, CP6, A2, P9, P7, P3, Pz, P4, P8, P10, O1, Oz and O2 were included. When 64 and 128 channels were used, the layout of the electrodes was consistent with that depicted in the literature [44]. The sampling rate of the simulated EEG signals was assigned as 256 Hz. For the extended source, we considered a patch generator which consisted of the adjacent grid dipoles with a radius of 15 cm [45]. Three chosen patches were located within the temporal lobe, namely: middle temporal (MT), inferior temporal (IT) and transverse temporal (TT) [46]. The center point coordinates of these patches were (-60.2, -13.7, 42.5), (-53.5, -5.80, 27.4), and (-61.8, 10.8, 57.5) mm. The current intensity of all dipoles on a patch generator was consistent with that of the above single dipole source. In the end, the WPESI algorithm was used to perform source reconstruction. The original sLORETA (OESI) method was also applied to the simulated EEG signals for comparison.

Source imaging accuracy was a primary concern in the ESI results. An ideal solution has the maximum strength source located at the exact position where the simulated test source is located [47]. In order to quantitatively assess the EEG source imaging accuracy for the single dipole source simulations, the selected criterion was the localization error, which was defined as the Euclidean distance from the estimated source with the maximum strength to the simulated source [48]. For the extended source simulations, the area under the ROC curve (AUC) was used to evaluate the concordance between the estimated current density distribution and the simulated source [46]. The larger the AUC value, the more consistent the overlap between the estimated source distribution and the extended source region.

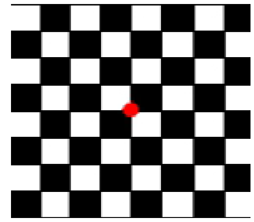

Fig. 2. Visual stimulation of black and white checkerboard.

2) VEP Data: Two subjects (age 19 and 21 years) took part in this study. Both subjects were healthy, male, and right-handed with normal vision. Written informed consent was obtained from the subjects before the experiments and the study was approved the 6 March 2012 by the Institutional Review Board at Xi'an Jiaotong University, China, ref. 2012-19. Fig. 2 depicts the visual stimulation of a black-and-white checkerboard used for the EEG experiments. In the EEG experiment, the pattern-reversal checkerboard was reversed at 1 Hz. The distance between the eyes and the stimulus screen was 1 m. Subjects were asked to maintain a comfortable eye position and to gaze at the central red fixation point during the EEG recordings. The VEP experiments were conducted in five trials. In each trial, the black-and-white checkerboard was reversed 60 consecutive times. The scalp EEG data were recorded with a SynAmps2 amplifier (Neuroscan Systems, Compumedics, Charlotte, NC, USA) from 32 scalp electrodes placed according to the standard 10-10 system. The channel Cz at the top of the head was used as the reference electrode. Differential amplifiers with band-pass filters between 0.02 and 100 Hz were used to minimize the effects of high-frequency noise and low-frequency artifact. The sampling frequency was 256 Hz.

Firstly, visible ocular blink and artifact rejection, band-pass filtering between 1 and 35 Hz, and segmentation with respect to stimulus onset were performed. After each VEP epoch was segmented based on trigger signals recorded during the recording session, pre-stimulus baseline correction and linear trend removal were sequentially applied to the segmented epochs. Bad channels, including unexpected distortions or fluctuations, were manually discarded based on visual examination of each channel of the EEG signal. In the end, 200 VEP epochs were selected and averaged to obtain the V200 signals. Unlike the simulated sources, there was a lack of ground truth for the cortical sources of the VEP signals. For the sLORETA method, if the signal does not have any noise, the localization error is zero [47]. Because the V200 signal was obtained by averaging 200 VEP signals, this signal had a high SNR. Hence, according to the P100 components of V200 signals, the maximum strength source estimated by sLORETA was regarded as the reference source. In addition, 80, 40 and 20 epochs were randomly selected from the total 200 VEP epochs. These epochs were averaged to obtain the new VEP signals V80, V40 and V20. Source imaging was performed

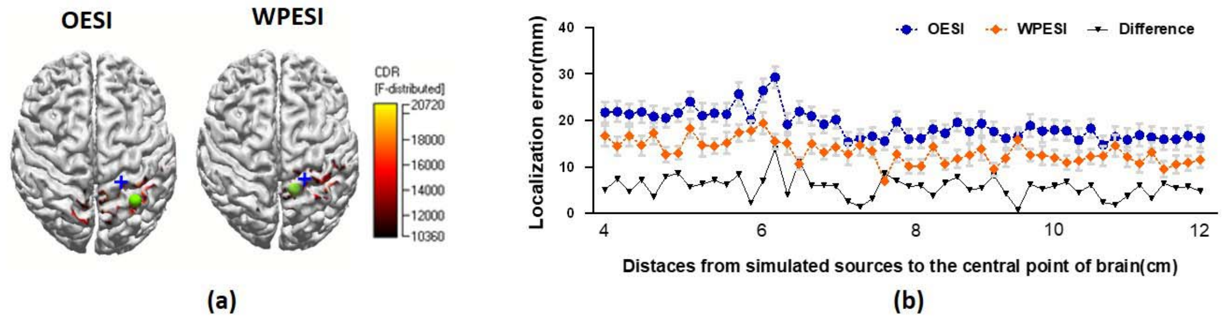

Fig. 3. (a) A typical example of source imaging results using the WPESI and OESI method for a single dipole source in the computer simulation. The green spheres identify the location of the estimated dipole source with the maximum strength, while the blue crosses represent the location of the simulated dipole source. The source imaging results are shown with a threshold of 50% maximum strength. (b) Comparison of localization errors between the WPESI and OESI methods at 50 different dipole sources when considering the simulated EEG signals contaminated by 200-times randomly generated GWN. The orange square and the blue circle represent the mean localization errors of each simulated source when using the WPESI method and OESI method, respectively. The vertical lines represent the standard error of the localization errors of each simulated source. The black triangles represent the differences between the localization errors of the WPESI and the OESI algorithms.

on the P100 component of V80, V40 and V20 by means of the WPESI and OESI methods. The localization error in this experiment was defined as the Euclidean distance from the estimated source with the maximum strength to the reference source. The localization errors of V80, V40 and V20 to the reference sources were then calculated. This process was randomly repeated 20 times. In order to verify the effectiveness of the WPESI method, the localization errors of two methods were compared in this study.

3) Epileptic EEG Data: The epileptic EEG data were derived from a public dataset (http://eeg.pl/epi/) containing a collection of patients diagnosed with refractory epilepsy who underwent surgical treatment at the Warsaw Memorial Child Hospital [49]. All patients were asked to be in the resting state. The 19-electrode montage was configured according to the standard 10-20 system in this experiment. The EEG signals, including interictal spikes, were acquired for 20 to 70 minutes before surgery using a Medelec-Profile system. The signal sampling rate was 256 Hz. In order to reduce the effects of artifact noise, the original data were preprocessed by a 0.5-70 Hz band-pass filter and a 50 Hz notch filter. The reference electrode of the hardware was Fpz. The MRI data, which contained T1-, T2- or FLAIR-weighted brain scan images, was scanned using a Siemens Sonata 1.5T machine. By examining intraoperative ECoG signals and postoperative recovery, the location of the epileptogenic zone was marked in the cross-sectional, coronal plane and sagittal planes of the preoperative MRI images. In order to keep the integrality of the EEG data and MRI data, three patients were selected to verify the effectiveness of the WPESI algorithm. The clinical information for these patients is summarized in TABLE I. The peaks of the averaged epileptic spikes for each patient were used for source estimation.

C. Statistical Analysis

For the same simulation source, a paired t-test was used to statistically compare the localization errors and the AUC indices between the WPESI and OESI methods. A value of $p<0.05$ was taken to indicate a statistically significant difference. In this study, all statistical analyses were performed with SPSS 25 (IBM; Chicago, IL, USA).

III. Results

A. Result of Computer Simulation Experiments

1) Effect of Different Simulation Source Locations: For each dipole source, 64 channels of simulated scalp EEG signals with 10 SNR of GWN were selected to perform source reconstruction with the WPESI and OESI algorithms. The numerical differences between the source localization results of the WPESI method and the OESI method for dipole sources are shown in Fig. 3. It could be seen in Fig. 3(a) that the distance between the maximum strength source estimated by the OESI method and the simulated dipole source was 21.74 mm, while the WPESI algorithm had an improved localization error, with a distance of 14.77 mm. As shown in Fig. 3(b), the results of the WPESI algorithm were superior to those of the OESI algorithm for 50 different dipole sources (paired t-test, $p<0.05$). At the same time, the localization accuracy was improved with increased distances between the simulated sources and the central point of the brain for both the WPESI and OESI algorithms. This indicates that the localization errors of deep sources are higher than those of shallow sources for both methods.

2) Effect of Different SNRs of the Simulation Signals: The 50th simulated source, which had the smallest depth to the cortical surface among all 50 dipole sources, was used in this experiment. The 64-channel scalp EEG signals were simulated by superimposing GWN and pink noise signals with 5, 10, 15, and 20 SNRs, respectively. Fig. 4 illustrates the source imaging differences between the WPESI and OESI algorithms for different SNRs. When the EEG signals generated by a simulated source were contaminated by the GWN signals with 5, 10, 15, and 20 SNRs, the mean localization errors of the WPESI method were 13.37, 11.03, 7.62, and 9.58 mm, respectively (Fig. 4(a)). However, the mean localization errors of the OESI method were 20.07, 16.67, 14.69 and 13.52 mm, respectively. Thus, the source imaging results of the WPESI

TABLE I
CLINICAL INFORMATION FOR THREE PATIENTS

Patient	Age	Gender	MRI findings	Surgery	Pathology	Outcome
GILPAU	15	Female	Signs of cortical dysplasia in left frontal lobe	Lesionectomy	Typical FCD with balloon cells (IIB) of left frontal lobe	Seizure free
HRADAW	12	Male	Typical picture of FCD within right frontal lobe	Broad resection of right frontal lobe	FCD type IIB	Seizure free
MARPAW	16	Male	Cystic tumor within mesiotemporal structures of right temporal lobe	Gross part of the right temporal lobe was removed	Complex form of dysebrioneuroepithelial tumor	Seizure free

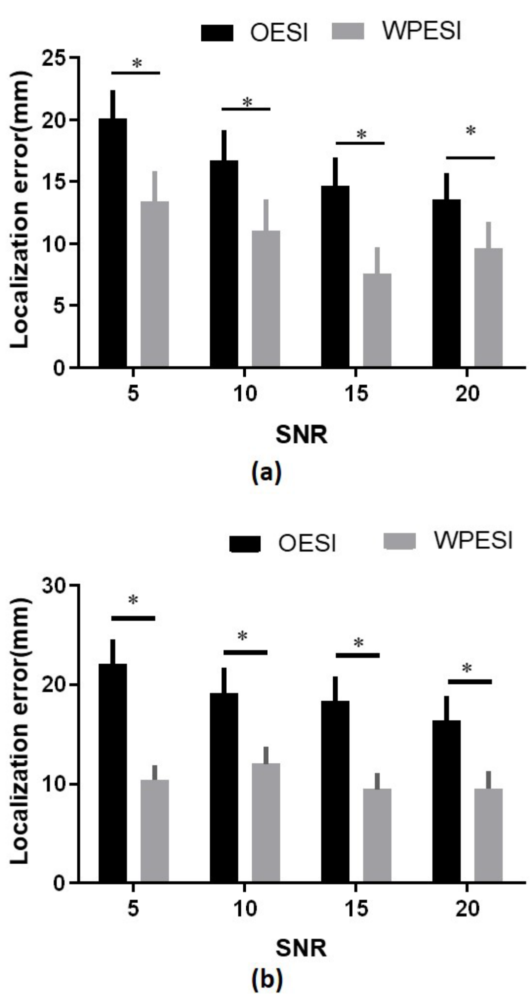

Fig. 4. Comparison of source imaging results for both WPESI and OESI algorithms using different SNRs of GWN (a) and pink noise (b) signals. The grey and black columns represent the mean values of the localization errors of the WPESI and OESI methods using the EEG signals with SNRs of 5, 10, 15 and 20, respectively. Bars: standard error. Asterisks indicate that the results of WPESI method are significantly better than those of OESI method.

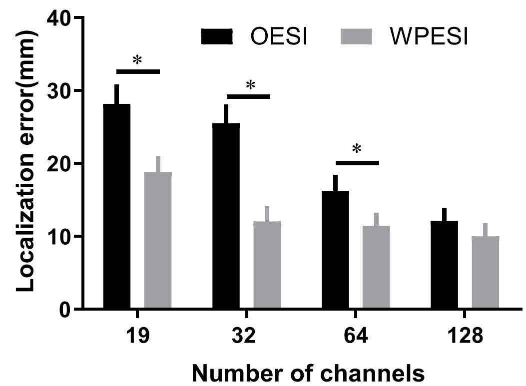

Fig. 5. Source imaging results under different electrode densities. The grey and black columns represent the mean values of the localization errors of the WPESI and OESI algorithms using 19, 32, 64 and 128 channels of EEG signals, respectively. Bars: standard error. Asterisks indicate that the results of the WPESI method are significantly better than those of the OESI method.

algorithm were superior to those of the OESI algorithm in the case of different SNRs (paired t-test, $p<0.05$). In addition, the localization accuracy of the OESI method was improved with increasing SNR (paired t-test, $p<0.05$). However, because there were no significant differences in the WPESI results between the 15 and 20 SNR signals, the localization accuracy of the WPESI algorithm was less affected by the SNR than the OESI algorithm. As shown in Fig. 4(b), the source imaging results using pink noise signals presented the same trend as evident in Fig. 4(a). These results indicate that the WPESI algorithm can be used in poor EEG experimental environments, rather than the OESI method.

3) Effect of Different Electrode Montages: The 50th simulated source and the GWN signals with 10 SNR were used to investigate the effect of different EEG electrode montages. Different algorithms were used to localize the 19, 32, 64, and 128 channels of simulated EEG signals. The comparison of the source imaging results under different electrode montages is shown in Fig. 5. It could be seen that the localization results of the WPESI algorithm were significantly better than those of the OESI algorithm for 19, 32 and 64 channels of EEG signals (paired t-test, $p<0.05$). Additionally, the localization accuracy of the OESI algorithm was significantly improved with an increasing number of electrodes. However, the localization error of the WPESI method was similar for the 32, 64 and 128 channels of signals (paired t-test, $p>0.05$), while these montages had significantly lower localization errors than the 19 channels of signals. These results indicate that the WPESI algorithm is hardly affected by the number of channels when the number of channels exceeds a certain value. Furthermore, the enhancement of localization accuracy using a low-density

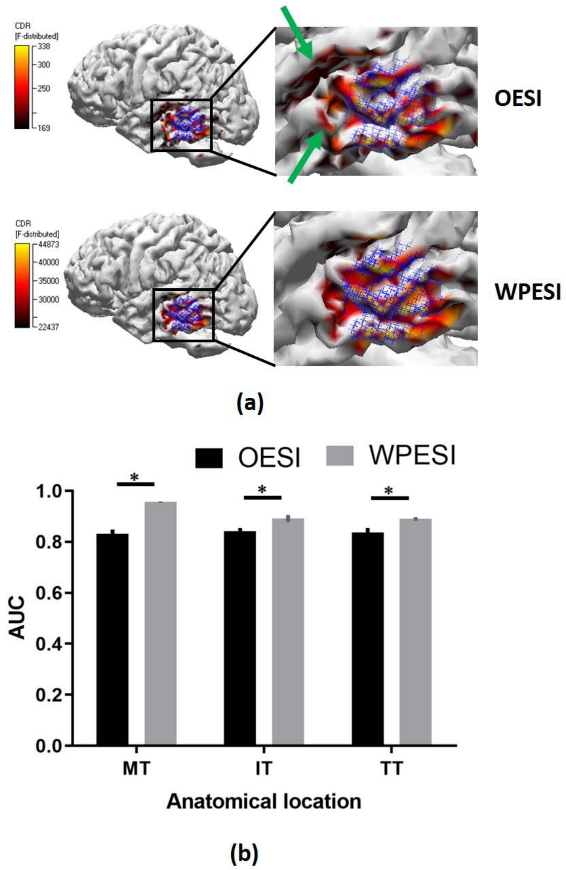

Fig. 6. (a) A typical example of source imaging results using the WPESI and OESI methods for an extended source simulated in the MT lobe. A zoomed view of the MT lobe is provided to better view the source imaging results. The red-yellow activation region on the cortex denotes the estimated current density distribution, while the blue crosses represent the extended simulation sources. The green arrows present the obvious differences between the extended sources estimated by the OESI and WPESI methods. The source imaging results are shown with a threshold of 50% maximum strength. (b) Comparison of AUC indices between the WPESI and OESI methods for three different anatomical locations. Bars: standard error. Asterisks indicate that the results of the WPESI method are significantly higher than those of the OESI method.

montage was much higher than that using a high-density montage for the WPESI algorithm. Hence, the proposed WPESI algorithm may be suitable for source imaging of scalp EEG signals under low-density electrode montages.

4) Extended Source Simulation Results: The 64-channel scalp EEG signals with 10 SNR of GWN were simulated for the extended sources that were located at the MT, IT and TT. The source imaging differences between the WPESI and OESI methods for the extended sources are illustrated in Fig. 6. It could be seen from Fig. 6(a) that the WPESI source imaging results were more concentrated on the simulated sources (blue crosses) than the OESI results, and the OESI distribution had spread to the neighboring cortical areas (green arrows). As shown in Fig. 6(b), the mean AUC indices for the three anatomical locations were 0.831, 0.841, and 0.836 for the OESI algorithm. When using the WPESI method, the mean AUC indices increased to 0.956, 0.891, and 0.889, respectively. The AUC indices of the WPESI method were significantly larger than those of the OESI method for all three extended sources (paired t-test, $p<0.05$). This demonstrates that the WPESI source imaging results are more concordant with the extended source region than the OESI results.

B. Results of the VEP Experiments

Because VEPs are relatively stable, there are many investigations that have used the ESI algorithm to explore the activation areas of the visual cortex [19], [50]. Therefore, visual cortex source imaging of the P100 was carried out and compared with the OESI algorithm. Fig. 7 shows the cortical current density distribution with the P100 of V20, V40 and V80 data for subject 1. It could be seen that the area of the current density distribution obtained by the OESI algorithm was large and relatively dispersed after averaging the VEP data 20 times. However, the current density distribution obtained by the WPESI algorithm was small and aggregated. After averaging the VEP data 40 times, the area of the current density distribution obtained by the OESI algorithm became smaller than that of V20. At the same time, the current density distribution obtained by the WPESI method was more concentrated in the occipital lobe than that obtained by the OESI method. The current density distribution of V80 was more focused than that of V20 and V40, regardless of whether the WPESI algorithm or OESI algorithm was used. Fig. 8 illustrates the localization errors between the reference sources and VEP sources when using V20, V40 and V80 EEG signals. Under the conditions of V80, V40 and V20, the localization errors of subject 1 obtained by the WPESI method were 6.35, 9.60 and 10.19 mm, respectively, and the localization errors obtained in subject 2 were 6.64, 8.64, and 11.85 mm, respectively. The localization accuracy of the OESI algorithm significantly worsened with a decreasing number of averaged VEP epochs while the WPESI algorithm was hardly affected by epoch number. There was no significant difference between the WPESI algorithm and the OESI algorithm in both subjects when the number of averaged VEP epochs was 80. However, when the number of averaged VEP epochs was 20 or 40, the source imaging accuracy of the WPESI algorithm was better than that of the OESI algorithm for both subjects (paired t-test, $p<0.05$). Averaging of EEG data is a commonly used method to improve the SNR of VEP signals. When the number of VEP epochs was small, the WPESI algorithm provided more accurate source imaging results than the OESI algorithm with localization errors within 10.19 and 11.85 mm from the reference source of the two subjects, respectively.

C. Results for Epilepsy Patients

The EEG source localization results of interictal spikes using the WPESI algorithm in epilepsy patient GILPAU are shown in Fig. 9. It could be seen that the EEG source localization results coincided with the clinical marked epileptic area. The source localization results using the WPESI algorithm in epilepsy patient HRADAW are illustrated in Fig. 10. The sources of the interictal spikes were in the right frontal lobe and clinical diagnosis indicated that the epileptogenic foci were also within the right frontal lobe. The EEG source

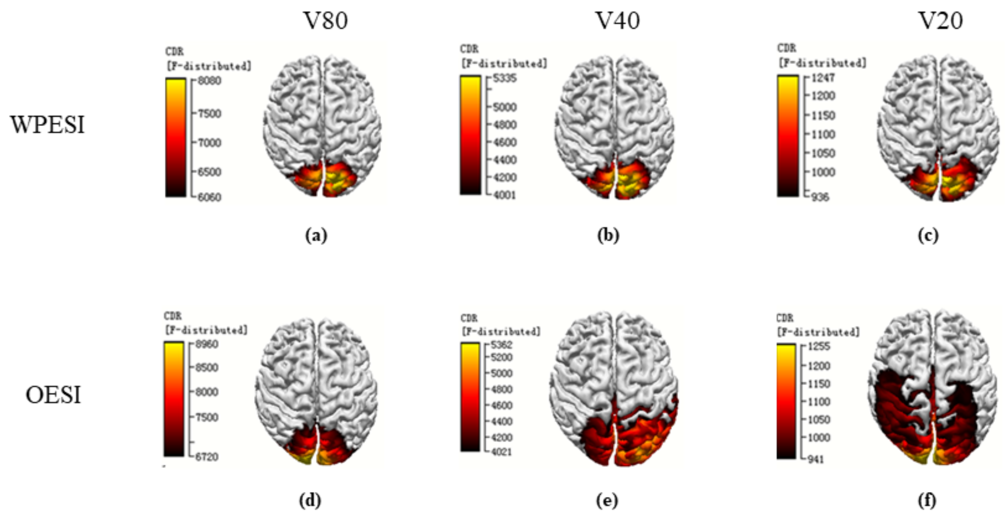

Fig. 7. The cortical current density distribution using the WPESI (a, b, c) and OESI (d, e, f) methods in subject 1 with P100 of V20 (c, f), V40 (b, e) and V80 (a, d). Colored bar denotes the strength of the current density distribution of the VEP signals. The source imaging results are shown with a threshold of 75% maximum strength.

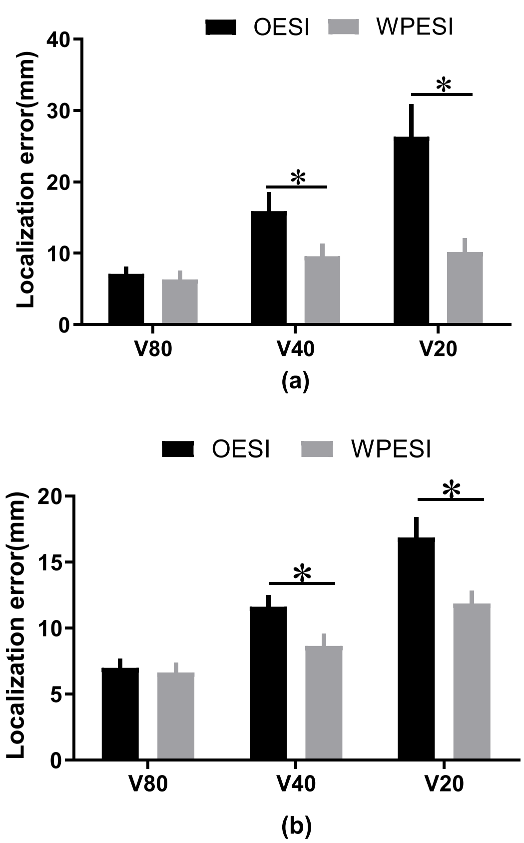

Fig. 8. The VEP source imaging results using the WPESI method and OESI methods with the P100 of V20, V40 and V80 data for subject 1 (a) and subject 2 (b). The grey and black columns represent the mean values of the localization errors of the WPESI and OESI methods. Bars: standard error. Asterisks indicate that the results of the WPESI method are significantly better than those of the OESI method.

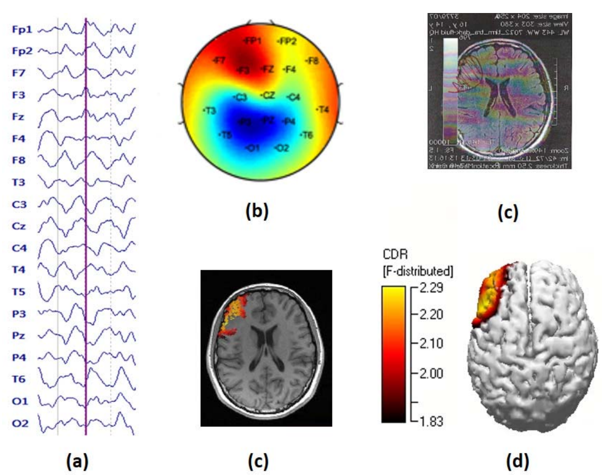

Fig. 9. The EEG source localization results of interictal spikes using the proposed algorithm in epilepsy patient GILPAU: (a) Interictal spikes in EEG signals; (b) The topography of the field distributions of interictal spikes; (c) Clinical diagnosis of epileptogenic zone of GILPAU; (d) Current density distribution of interictal spike projected on the axial plane; (e) 3D display of current density distribution of interictal spikes using the WPESI method; colored bar denotes the strength of the current density distribution. The source imaging results are shown with a threshold of 80% maximum strength.

localization results in epilepsy patient MARPAW are shown in Fig. 11. The MRI images indicated that benign tumors were within the right temporal lobe, which is similar to the WPESI results. Therefore, the clinical diagnosis results of epileptogenic lesions in these three epilepsy patients were consistent with the EEG source localization results provided by the WPESI algorithm.

IV. Discussion

A. Effectiveness of the WPESI Method

In this study, the aim of the proposed WPESI algorithm was to generate subspace components of EEG signals by means of wavelet packet decomposition. The selection of subspace components is actually the selection of frequency

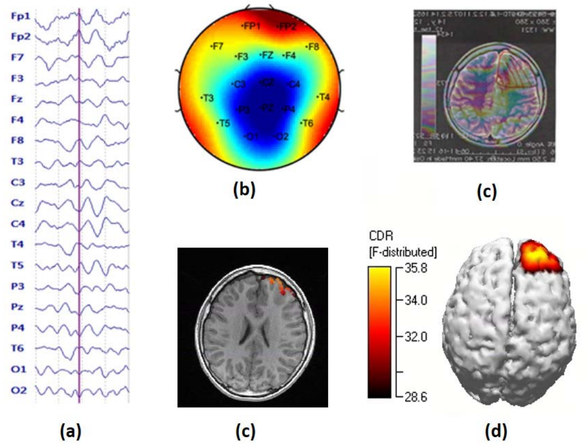

Fig. 10. The EEG source localization results of interictal spikes using the proposed algorithm in epilepsy patient HRADAW: (a) Interictal spikes in EEG signals; (b) The topography of the field distributions of interictal spikes; (c) Clinical diagnosis of epileptogenic zone of HRADAW; (d) Current density distribution of interictal spikes projected on the axial plane; (e) 3D display of the current density distribution of interictal spikes using the WPESI method; colored bar denotes the strength of the current density distribution. The source imaging results are shown with a threshold of 80% maximum strength.

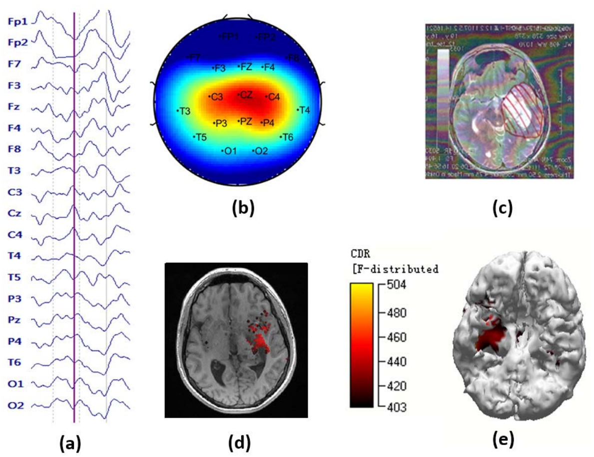

Fig. 11. The EEG source localization results of interictal spikes using the proposed algorithm in epilepsy patient MARPAW: (a) Interictal spikes in EEG signals; (b) The topography of the field distributions of interictal spikes; (c) Clinical diagnosis of epileptogenic zone of MARPAW; (d) Current density distribution of interictal spikes projected on the axial plane; (e) 3D display of the current density distribution of interictal spikes using the WPESI method; colored bar denotes the strength of the current density distribution. The source imaging results are shown with a threshold of 80% maximum strength.

bands. In raw EEG signals, many frequency components are probably independent of the source information. Therefore, if all frequency bands are applied to localizing the brain electrical source, then the localization results may not be accurate. If the frequency band that needs to be retained can be clearly identified, such as by analyzing a certain rhythm of EEG signals or eliminating noise from EEG signals, the subspace component corresponding to the fixed frequency band can be directly selected. However, if it is difficult to identify the frequency band that needs to be retained, such as in epilepsy-related EEG signals, the method of retaining a fixed

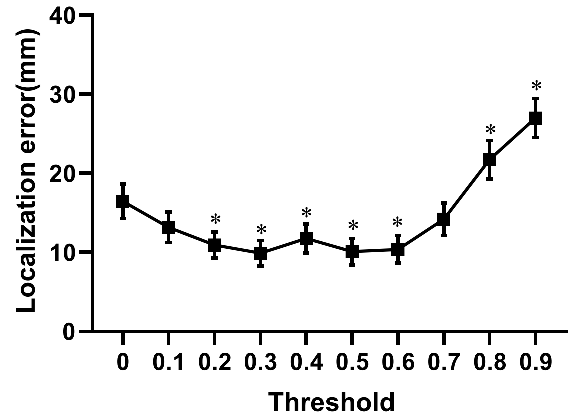

Fig. 12. The source imaging results of different thresholds used to select the subspace component. Each point represents the mean value of the localization error for different thresholds. Bars: standard error. Asterisks indicate that the results of the WPESI algorithm with various thresholds are significantly different from those of the OESI algorithm (threshold is zero).

frequency band to select the subspace component is unfeasible. The algorithm proposed in this study uses Pearson correlation analysis to select the subspace component according to the absolute value of the correlation coefficient. This component selection method can effectively extract the related frequency components from EEG signals and is resistant to noise and artifact. Therefore, source imaging accuracy is effectively improved with the use of the WPESI algorithm.

This method was tested in three experiments and achieved remarkable results. In addition to the EEG inverse algorithm, the position and direction of the brain source, the resolution of the head model, and the number of electrode channels are all related to the source imaging results. In the computer simulation, with increased SNR, the localization accuracy was improved, which is consistent with the results of previous studies [51]. In the VEP experiment, the current density distribution obtained with the WPESI method was more concentrated on the occipital visual cortex than that obtained with the OESI method at P100. With increased average times of the P100, the SNR of VEP signals was improved and the localization accuracy of the WPESI method at P100 showed improvement. According to the above results, given that the WPESI method can increase the SNR of source-related signals by means of WPT and subspace selection, this algorithm might improve the accuracy of EEG source localization.

The WPESI algorithm achieved lower localization error than the OESI method for deep simulated sources, as well as low SNR of EEG signals and low-density electrode montages. In the VEP source imaging experiments, the localization results of the WPESI algorithm were more accurate than those of the OESI method when the number of VEP epochs was small. There are many studies using high-density EEG to localize the seizure onset zone and good results have been obtained [15], [52]. However, the WPESI algorithm can use 19-channel EEG signals to identify the seizure onset zone.

B. Effect of Threshold in Subspace Component Selection

With the WPESI algorithm, multiple subspaces were firstly decomposed by WPT. Then, the relevant subspaces were selected and reconstructed. In the end, the reconstructed EEG signal was used for ESI. The selection of subspace components depended on the threshold of the correlation coefficient between the subspace component and the original EEG signal. Therefore, the threshold is very important for subspace component selection, and can also affect the ESI results. The 50th simulated source was chosen to evaluate the different thresholds. Fig. 12 shows a comparison of the localization results for different thresholds that were used to select the subspace component. When the threshold was zero, the WPESI method was the same as the OESI method. In this figure, it could be seen that when the threshold ranged from 0.2 to 0.6, the localization errors of the WPESI method were significantly smaller than those of the OESI method (paired t-test, $p<0.05$). Hence, a threshold in this range should be chosen. When the threshold was set to 0.7, there was no significant difference between the WPESI and OESI methods for the source imaging results. However, when the threshold was greater than 0.7, the localization errors of the WPESI algorithm were larger than those of the OESI method (paired t-test, $p<0.05$). This is because the threshold is so high that most subspaces are filtered out and useful EEG signals are eliminated, resulting in poor source imaging results. In addition, there was no significant difference in the localization results with thresholds of 0.2, 0.3, 0.4, 0.5, or 0.6. Therefore, 0.5 was chosen as the constant threshold for the WPESI method in this study.

C. Comparison With Other Algorithms

Although the sLORETA method has low spatial resolution, it is a commonly used method in EEG source imaging [41]–[43]. Compared with the original sLORETA, the proposed WPESI method achieved satisfactory source imaging results. To further discuss the performance of the proposed method, this method was compared with two other existing algorithms: the SWARM [53] and L1 norm methods [54]. The SWARM (sLORETA-weighted accurate minimum norm inverse solutions) method is a weighted minimum norm solution with its weights based on sLORETA. In addition to the L2 norm regularization, L1 norm regularization tends to yield more sparse solutions. Both the single dipole source and the extended source were used to analyze the performance of the different methods in the computer simulation experiments. The configurations of the single dipole source and the extended source were the same as those in the computer simulation data. For the single dipole source, the 50th source in all simulated dipoles was used. The extended source was located within the TT lobe. Fig. 13 shows the numerical differences among source localization accuracies of the different ESI approaches when using the single dipole source and the extended source. For the single dipole source, the mean localization error of the WPESI algorithm was nearly 4 mm smaller than that of the OESI algorithm, and approximately 24 mm smaller than that of the L1 norm method. There was no significant difference in localization error between the WPESI and the SWARM methods. For the extended source, the mean AUC index of the source imaging results using the WPESI method

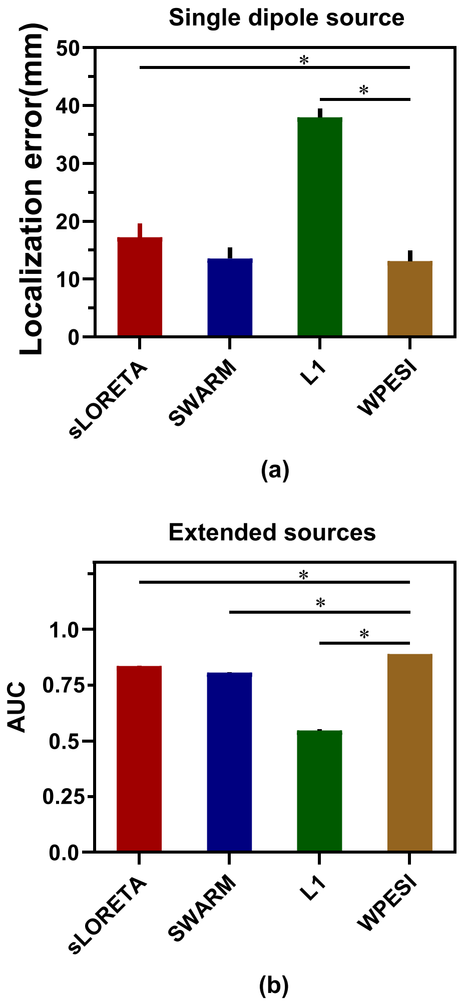

Fig. 13. Comparison of localization errors and AUC indices among the different ESI methods using the single dipole source (a) and the extended source (b). Bars: standard error. Asterisks indicate that the results of the WPESI method are significantly different from those of the other method.

was significantly higher than those obtained with the other three methods (paired t-test, $p<0.05$).

D. Limitations and Future Work

There are some limitations of this study that should be noted. In the computer simulation experiments, multiple dipole sources can be considered at the same time. In the VEP experiments, the dipole with the maximum strength among the cortical surface sources related to the P100 components of V200 signals was chosen as the reference source, because the localization error was very small when the SNR was very high. Although the P100 component of V200 signals had a high SNR level, the location of the reference source was not the ground truth of the P100 source. Besides WPT, there are several other novel subspace decomposition approaches, such as symplectic geometry spectrum [55], fuzzy singular spectrum [56], and so on. These algorithms can be used to further improve the accuracy of EEG source imaging. In some recent investigations, the FAST-IRES algorithm [57], the tensor-based source localization [58], and the MEM-type optimization [31] were proposed for extended source imaging. The exhaustive comparison of the WPESI results to these existing techniques is also essential for future studies.

V. Conclusion

In this paper, a new WPESI method was proposed and used in computer simulation experiments and VEP experiments. It was also then used for EEG source localization among patients with epilepsy. In the computer simulation experiments, the localization ability of the proposed WPESI method was superior to that of the original sLORETA method, especially for deep simulated sources, simulated EEG signals with low SNR, signals obtained with low-density electrode montages, and extended sources. In the VEP source imaging experiments, the WPESI algorithm provided higher accuracy than the original sLORETA method when the number of VEP epochs was small. For patients with medically intractable epilepsy, the use of the WPESI algorithm on interictal spikes was able to effectively localize the epileptogenic foci. These results demonstrate that the proposed WPESI method exhibits better localization accuracy than the original sLORETA method. Therefore, this method could be applied to localize epileptic foci in epilepsy patients.

References

[1] N. von Ellenrieder, L. Beltrachini, P. Perucca, and J. Gotman, "Size of cortical generators of epileptic interictal events and visibility on scalp EEG," *NeuroImage*, vol. 94, pp. 47–54, Jul. 2014.

[2] J. X. Tao, A. Ray, S. Hawes-Ebersole, and J. S. Ebersole, "Intracranial EEG substrates of scalp EEG interictal spikes," *Epilepsia*, vol. 46, no. 5, pp. 669–676, May 2005.

[3] S.-H. Hsu, T. R. Mullen, T.-P. Jung, and G. Cauwenberghs, "Real-time adaptive EEG source separation using online recursive independent component analysis," *IEEE Trans. Neural Syst. Rehabil. Eng.*, vol. 24, no. 3, pp. 309–319, Mar. 2016.

[4] Q. Wang and O. Sourina, "Real-time mental arithmetic task recognition from EEG signals," *IEEE Trans. Neural Syst. Rehabil. Eng.*, vol. 21, no. 2, pp. 225–232, Mar. 2013.

[5] D. Wang *et al.*, "Epileptic seizure detection in long-term EEG recordings by using wavelet-based directed transfer function," *IEEE Trans. Biomed. Eng.*, vol. 65, no. 11, pp. 2591–2599, Nov. 2018.

[6] G. Wang, Z. Sun, R. Tao, K. Li, G. Bao, and X. Yan, "Epileptic seizure detection based on partial directed coherence analysis," *IEEE J. Biomed. Health Inform.*, vol. 20, no. 3, pp. 873–879, May 2016.

[7] Y. Zheng, G. Wang, K. Li, G. Bao, and J. Wang, "Epileptic seizure prediction using phase synchronization based on bivariate empirical mode decomposition," *Clin. Neurophysiol.*, vol. 125, no. 6, pp. 1104–1111, Jun. 2014.

[8] Y. Park, L. Luo, K. K. Parhi, and T. Netoff, "Seizure prediction with spectral power of EEG using cost-sensitive support vector machines," *Epilepsia*, vol. 52, no. 10, pp. 1761–1770, Oct. 2011.

[9] G. Wang *et al.*, "Seizure prediction using directed transfer function and convolution neural network on intracranial EEG," *IEEE Trans. Neural Syst. Rehabil. Eng.*, vol. 28, no. 12, pp. 2711–2720, Dec. 2020.

[10] M. De Vos *et al.*, "Canonical decomposition of ictal scalp EEG reliably detects the seizure onset zone," *NeuroImage*, vol. 37, no. 3, pp. 844–854, Sep. 2007.

[11] J. C. Mosher and R. M. Leahy, "Source localization using recursively applied and projected (RAP) MUSIC," *IEEE Trans. Signal Process.*, vol. 47, no. 2, pp. 332–340, Feb. 1999.

[12] L. Ding, G. A. Worrell, T. D. Lagerlund, and B. He, "Ictal source analysis: Localization and imaging of causal interactions in humans," *NeuroImage*, vol. 34, no. 2, pp. 575–586, Jan. 2007.

[13] R. D. Pascual-Marqui, C. M. Michel, and D. Lehmann, "Low resolution electromagnetic tomography: A new method for localizing electrical activity in the brain," *Int. J. Psychophysiol.*, vol. 18, no. 1, pp. 49–65, Oct. 1994.

[14] I. F. Gorodnitsky, J. S. George, and B. D. Rao, "Neuromagnetic source imaging with FOCUSS: A recursive weighted minimum norm algorithm," *Electroencephalogr. Clin. Neurophysiol.*, vol. 95, no. 4, pp. 231–251, Oct. 1995.

[15] G. Wang, G. Worrell, L. Yang, C. Wilke, and B. He, "Interictal spike analysis of high-density EEG in patients with partial epilepsy," *Clin. Neurophysiol.*, vol. 122, no. 6, pp. 1098–1105, Jun. 2011.

[16] V. Brodbeck, A. M. Lascano, L. Spinelli, M. Seeck, and C. M. Michel, "Accuracy of EEG source imaging of epileptic spikes in patients with large brain lesions," *Clin. Neurophysiol.*, vol. 120, no. 4, pp. 679–685, Apr. 2009.

[17] D. Rathee, H. Raza, G. Prasad, and H. Cecotti, "Current source density estimation enhances the performance of motor-imagery-related brain–computer interface," *IEEE Trans. Neural Syst. Rehabil. Eng.*, vol. 25, no. 12, pp. 2461–2471, Dec. 2017.

[18] N. Yan *et al.*, "Quadcopter control system using a hybrid BCI based on off-line optimization and enhanced human-machine interaction," *IEEE Access*, vol. 8, pp. 1160–1172, 2020.

[19] C.-H. Im, A. Gururajan, N. Zhang, W. Chen, and B. He, "Spatial resolution of EEG cortical source imaging revealed by localization of retinotopic organization in human primary visual cortex," *J. Neurosci. Methods*, vol. 161, no. 1, pp. 142–154, Mar. 2007.

[20] W. Staljanssens *et al.*, "EEG source connectivity to localize the seizure onset zone in patients with drug resistant epilepsy," *NeuroImage, Clin.*, vol. 16, pp. 689–698, 2017.

[21] C.-C. Kuo *et al.*, "EEG source imaging of epileptic activity at seizure onset," *Epilepsy Res.*, vol. 146, pp. 160–171, Oct. 2018.

[22] V. Rimpiläinen, A. Koulouri, F. Lucka, J. P. Kaipio, and C. H. Wolters, "Improved EEG source localization with Bayesian uncertainty modelling of unknown skull conductivity," *NeuroImage*, vol. 188, pp. 252–260, Mar. 2019.

[23] N. Mäkelä, M. Stenroos, J. Sarvas, and R. J. Ilmoniemi, "Truncated RAP-MUSIC (TRAP-MUSIC) for MEG and EEG source localization," *NeuroImage*, vol. 167, pp. 73–83, Feb. 2018.

[24] S. Machado *et al.*, "Source imaging of P300 visual evoked potentials and cognitive functions in healthy subjects," *Clin. EEG Neurosci.*, vol. 45, no. 4, pp. 262–268, Oct. 2014.

[25] T. Hedrich, G. Pellegrino, E. Kobayashi, J. M. Lina, and C. Grova, "Comparison of the spatial resolution of source imaging techniques in high-density EEG and MEG," *NeuroImage*, vol. 157, pp. 531–544, Aug. 2017.

[26] S. U. Schuele and H. O. Lüders, "Intractable epilepsy: Management and therapeutic alternatives," *Lancet Neurol.*, vol. 7, no. 6, pp. 514–524, Jun. 2008.

[27] F. Rosenow and H. Luders, "Presurgical evaluation of epilepsy," *Brain*, vol. 124, no. 9, pp. 1683–1700, Sep. 2001.

[28] D. Lai *et al.*, "Automated detection of high frequency oscillations in intracranial EEG using the combination of short-time energy and convolutional neural networks," *IEEE Access*, vol. 7, pp. 82501–82511, 2019.

[29] D. Lai *et al.*, "Channel-wise characterization of high frequency oscillations for automated identification of the seizure onset zone," *IEEE Access*, vol. 8, pp. 45531–45543, 2020.

[30] G. Pellegrino *et al.*, "Source localization of the seizure onset zone from ictal EEG/MEG data," *Hum. Brain Mapping*, vol. 37, no. 7, pp. 2528–2546, Jul. 2016.

[31] M. Heers *et al.*, "Localization accuracy of distributed inverse solutions for electric and magnetic source imaging of interictal epileptic discharges in patients with focal epilepsy," *Brain Topography*, vol. 29, no. 1, pp. 162–181, Jan. 2016.

[32] L. Yang, C. Wilke, B. Brinkmann, G. A. Worrell, and B. He, "Dynamic imaging of ictal oscillations using non-invasive high-resolution EEG," *NeuroImage*, vol. 56, no. 4, pp. 1908–1917, Jun. 2011.

[33] C. Li *et al.*, "Epileptogenic source imaging using cross-frequency coupled signals from scalp EEG," *IEEE Trans. Biomed. Eng.*, vol. 63, no. 12, pp. 2607–2618, Dec. 2016.

[34] V. Brodbeck *et al.*, "Electroencephalographic source imaging: A prospective study of 152 operated epileptic patients," *Brain*, vol. 134, no. 10, pp. 2887–2897, Oct. 2011.

[35] M. Gavaret *et al.*, "Source localization of scalp-EEG interictal spikes in posterior cortex epilepsies investigated by HR-EEG and SEEG," *Epilepsia*, vol. 50, no. 2, pp. 276–289, Jan. 2009.

[36] G. Strobbe *et al.*, "Electrical source imaging of interictal spikes using multiple sparse volumetric priors for presurgical epileptogenic focus localization," *NeuroImage, Clin.*, vol. 11, pp. 252–263, Jan. 2016.

[37] A. Coito *et al.*, “Interictal epileptogenic zone localization in patients with focal epilepsy using electric source imaging and directed functional connectivity from low-density EEG,” *Epilepsia Open*, vol. 4, no. 2, pp. 281–292, Jun. 2019.

[38] A. S. Zandi, M. Javidan, G. A. Dumont, and R. Tafreshi, “Automated real-time epileptic seizure detection in scalp EEG recordings using an algorithm based on wavelet packet transform,” *IEEE Trans. Biomed. Eng.*, vol. 57, no. 7, pp. 1639–1651, Jul. 2010.

[39] G. Wang and D. Ren, “Effect of brain-to-skull conductivity ratio on EEG source localization accuracy,” *BioMed Res. Int.*, vol. 2013, pp. 1–10, Apr. 2013.

[40] R. D. Pascual-Marqui, “Standardized low-resolution brain electromagnetic tomography (sLORETA): Technical details,” *Methods Find Exp. Clin. Pharmacol.*, vol. 24, no. 2, pp. 5–12, Jan. 2002.

[41] C. Beste, C. Saft, J. Andrich, R. Gold, and M. Falkenstein, “Response inhibition in Huntington’s disease—A study using ERPs and sLORETA,” *Neuropsychologia*, vol. 46, no. 5, pp. 1290–1297, 2008.

[42] J. R. Tenney, H. Fujiwara, P. S. Horn, and D. F. Rose, “Comparison of magnetic source estimation to intracranial EEG, resection area, and seizure outcome,” *Epilepsia*, vol. 55, no. 11, pp. 1854–1863, Nov. 2014.

[43] M. Yazici, M. Ulutas, and M. Okuyan, “A comprehensive sLORETA study on the contribution of cortical somatomotor regions to motor imagery,” *Brain Sci.*, vol. 9, no. 12, p. 372, Dec. 2019.

[44] R. Oostenveld and P. Praamstra, “The five percent electrode system for high-resolution EEG and ERP measurements,” *Clin. Neurophysiol.*, vol. 112, no. 4, pp. 713–719, Apr. 2001.

[45] P. Xu, Y. Tian, H. Chen, and D. Yao, “Lp norm iterative sparse solution for EEG source localization,” *IEEE Trans. Biomed. Eng.*, vol. 54, no. 3, pp. 400–409, Mar. 2007.

[46] C. Grova, J. Daunizeau, J.-M. Lina, C. G. Bénar, H. Benali, and J. Gotman, “Evaluation of EEG localization methods using realistic simulations of interictal spikes,” *NeuroImage*, vol. 29, no. 3, pp. 734–753, Feb. 2006.

[47] H. Liu, X. Gao, P. H. Schimpf, F. Yang, and S. Gao, “A recursive algorithm for the three-dimensional imaging of brain electric activity: Shrinking LORETA-FOCUSS,” *IEEE Trans. Biomed. Eng.*, vol. 51, no. 10, pp. 1794–1802, Oct. 2004.

[48] D. Cosandier-Rimélé, G. Ramantani, J. Zentner, A. Schulze-Bonhage, and M. Dümpelmann, “A realistic multimodal modeling approach for the evaluation of distributed source analysis: Application to sLORETA,” *J. Neural Eng.*, vol. 14, no. 5, Oct. 2017, Art. no. 056008.

[49] P. Zwolinski, M. Roszkowski, J. Zygierewicz, S. Haufe, G. Nolte, and P. J. Durka, “Open database of epileptic EEG with MRI and postoperational assessment of foci—A real world verification for the EEG inverse solutions,” *Neuroinformatics*, vol. 8, no. 4, pp. 285–299, Dec. 2010.

[50] K. Whittingstall, G. Stroink, and M. Schmidt, “Evaluating the spatial relationship of event-related potential and functional MRI sources in the primary visual cortex,” *Hum. Brain Mapping*, vol. 28, no. 2, pp. 134–142, Feb. 2007.

[51] O. Hauk, D. G. Wakeman, and R. Henson, “Comparison of noise-normalized minimum norm estimates for MEG analysis using multiple resolution metrics,” *NeuroImage*, vol. 54, no. 3, pp. 1966–1974, Feb. 2011.

[52] W. Staljanssens *et al.*, “Seizure onset zone localization from ictal high-density EEG in refractory focal epilepsy,” *Brain Topography*, vol. 30, no. 2, pp. 257–271, Mar. 2017.

[53] M. Wagner, M. Fuchs, and J. Kastner, “SWARM: SLORETA-weighted accurate minimum norm inverse solutions,” *Int. Congr. Ser.*, vol. 1300, pp. 185–188, Jun. 2007.

[54] X. Bai, V. L. Towle, E. J. He, and B. He, “Evaluation of cortical current density imaging methods using intracranial electrocorticograms and functional MRI,” *NeuroImage*, vol. 35, no. 2, pp. 598–608, Apr. 2007.

[55] H.-B. Xie, T. Guo, B. Sivakumar, A. W.-C. Liew, and S. Dokos, “Symplectic geometry spectrum analysis of nonlinear time series,” *Proc. Roy. Soc. A, Math., Phys. Eng. Sci.*, vol. 470, no. 2170, Oct. 2014, Art. no. 20140409.

[56] H.-B. Xie, B. Sivakumar, T. W. Boonstra, and K. Mengersen, “Fuzzy entropy and its application for enhanced subspace filtering,” *IEEE Trans. Fuzzy Syst.*, vol. 26, no. 4, pp. 1970–1982, Aug. 2018.

[57] A. Sohrabpour, Z. Cai, S. Ye, B. Brinkmann, G. Worrell, and B. He, “Noninvasive electromagnetic source imaging of spatiotemporally distributed epileptogenic brain sources,” *Nature Commun.*, vol. 11, no. 1, pp. 1–15, Dec. 2020.

[58] H. Becker *et al.*, “EEG extended source localization: Tensor-based vs. Conventional methods,” *NeuroImage*, vol. 96, pp. 143–157, Aug. 2014.